Biomedical Optics EXPRESS

Adaptive optics two-photon excited fluorescence lifetime imaging ophthalmoscopy of exogenous fluorophores in mice

JAMES A. FEEKS[1,2,*] **AND JENNIFER J. HUNTER**[1,3,4]

[1] *Center for Visual Science, University of Rochester, Rochester, NY 14627, USA*
[2] *The Institute of Optics, University of Rochester, Rochester, NY 14620, USA*
[3] *Flaum Eye Institute, University of Rochester, NY 14642, USA*
[4] *Department of Biomedical Engineering, University of Rochester, NY 14627, USA*
[*] *jfeeks@ur.rochester.edu*

Abstract: *In vivo* cellular scale fluorescence lifetime imaging of the mouse retina has the potential to be a sensitive marker of retinal cell health. In this study, we demonstrate fluorescence lifetime imaging of extrinsic fluorophores using adaptive optics fluorescence lifetime imaging ophthalmoscopy (AOFLIO). We recorded AOFLIO images of inner retinal cells labeled with enhanced green fluorescent protein (EGFP) and capillaries labeled with fluorescein. We demonstrate that AOFLIO can be used to differentiate spectrally overlapping fluorophores in the retina. With further refinements, AOFLIO could be used to assess retinal health in early stages of degeneration by utilizing lifetime-based sensors or even fluorophores native to the retina.

OCIS codes: (170.4460) Ophthalmic optics and devices; (170.0110) Imaging systems; (170.3650) Lifetime-based sensing; (110.1080) Active or adaptive optics.

References and links

1. E. A. Rossi, P. Rangel-Fonseca, K. Parkins, W. Fischer, L. R. Latchney, M. A. Folwell, D. R. Williams, A. Dubra, and M. M. Chung, "In vivo imaging of retinal pigment epithelium cells in age related macular degeneration," Biomed. Opt. Express **4**(11), 2527–2539 (2013).
2. Y. Geng, A. Dubra, L. Yin, W. H. Merigan, R. Sharma, R. T. Libby, and D. R. Williams, "Adaptive optics retinal imaging in the living mouse eye," Biomed. Opt. Express **3**(4), 715–734 (2012).
3. D. J. Wahl, Y. Jian, S. Bonora, R. J. Zawadzki, and M. V. Sarunic, "Wavefront sensorless adaptive optics fluorescence biomicroscope for in vivo retinal imaging in mice," Biomed. Opt. Express **7**(1), 1–12 (2015).
4. J. Tam, J. Liu, A. Dubra, and R. Fariss, "In Vivo Imaging of the Human Retinal Pigment Epithelial Mosaic Using Adaptive Optics Enhanced Indocyanine Green Ophthalmoscopy," Invest. Ophthalmol. Vis. Sci. **57**(10), 4376–4384 (2016).
5. J. I. W. Morgan, A. Dubra, R. Wolfe, W. H. Merigan, and D. R. Williams, "In Vivo Autofluorescence Imaging of the Human and Macaque Retinal Pigment Epithelial Cell Mosaic," Invest. Ophthalmol. Vis. Sci. **50**(3), 1350–1359 (2009).
6. A. Pinhas, M. Dubow, N. Shah, T. Y. Chui, D. Scoles, Y. N. Sulai, R. Weitz, J. B. Walsh, J. Carroll, A. Dubra, and R. B. Rosen, "In vivo imaging of human retinal microvasculature using adaptive optics scanning light ophthalmoscope fluorescein angiography," Biomed. Opt. Express **4**(8), 1305–1317 (2013).
7. G. Palczewska, Z. Dong, M. Golczak, J. J. Hunter, D. R. Williams, N. S. Alexander, and K. Palczewski, "Noninvasive two-photon microscopy imaging of mouse retina and retinal pigment epithelium through the pupil of the eye," Nat. Med. **20**(7), 785–789 (2014).
8. R. Sharma, L. Yin, Y. Geng, W. H. Merigan, G. Palczewska, K. Palczewski, D. R. Williams, and J. J. Hunter, "In vivo two-photon imaging of the mouse retina," Biomed. Opt. Express **4**(8), 1285–1293 (2013).
9. J. J. Hunter, B. Masella, A. Dubra, R. Sharma, L. Yin, W. H. Merigan, G. Palczewska, K. Palczewski, and D. R. Williams, "Images of photoreceptors in living primate eyes using adaptive optics two-photon ophthalmoscopy," Biomed. Opt. Express **2**(1), 139–148 (2010).
10. R. Sharma, D. R. Williams, G. Palczewska, K. Palczewski, and J. J. Hunter, "Two-Photon Autofluorescence Imaging Reveals Cellular Structures Throughout the Retina of the Living Primate Eye," Invest. Ophthalmol. Vis. Sci. **57**(2), 632–646 (2016).

#283011 https://doi.org/10.1364/BOE.8.002483
Journal © 2017 Received 4 Jan 2017; revised 7 Apr 2017; accepted 7 Apr 2017; published 17 Apr 2017

11. L. Yin, Y. Geng, F. Osakada, R. Sharma, A. H. Cetin, E. M. Callaway, D. R. Williams, and W. H. Merigan, "Imaging light responses of retinal ganglion cells in the living mouse eye," J. Neurophysiol. **109**(9), 2415–2421 (2013).
12. L. Yin, B. Masella, D. Dalkara, J. Zhang, J. G. Flannery, D. V. Schaffer, D. R. Williams, and W. H. Merigan, "Imaging Light Responses of Foveal Ganglion Cells in the Living Macaque Eye," J. Neurosci. **34**(19), 6596–6605 (2014).
13. R. Sharma, C. Schwarz, D. R. Williams, G. Palczewska, K. Palczewski, and J. J. Hunter, "In Vivo Two-Photon Fluorescence Kinetics of Primate Rods and Cones," Invest. Ophthalmol. Vis. Sci. **57**(2), 647–657 (2016).
14. F. Delori, J. P. Greenberg, R. L. Woods, J. Fischer, T. Duncker, J. Sparrow, and R. T. Smith, "Quantitative measurements of autofluorescence with the scanning laser ophthalmoscope," Invest. Ophthalmol. Vis. Sci. **52**(13), 9379–9390 (2011).
15. J. R. Lakowicz, *Principles of Fluorescence Spectroscopy* (Springer Science + Business Media, 2006).
16. M. Tantama, Y. P. Hung, and G. Yellen, "Imaging intracellular pH in live cells with a genetically encoded red fluorescent protein sensor," J. Am. Chem. Soc. **133**(26), 10034–10037 (2011).
17. D. Schweitzer, M. Hammer, F. Schweitzer, R. Anders, T. Doebbecke, S. Schenke, E. R. Gaillard, and E. R. Gaillard, "In vivo measurement of time-resolved autofluorescence at the human fundus," J. Biomed. Opt. **9**(6), 1214–1222 (2004).
18. D. Schweitzer, S. Schenke, M. Hammer, F. Schweitzer, S. Jentsch, E. Birckner, W. Becker, and A. Bergmann, "Towards metabolic mapping of the human retina," Microsc. Res. Tech. **70**(5), 410–419 (2007).
19. C. Dysli, M. Dysli, V. Enzmann, S. Wolf, and M. S. Zinkernagel, "Fluorescence Lifetime Imaging of the Ocular Fundus in Mice," Invest. Ophthalmol. Vis. Sci. **55**(11), 7206–7215 (2014).
20. J. Dillon, L. Zheng, J. C. Merriam, and E. R. Gaillard, "Transmission spectra of light to the mammalian retina," Photochem. Photobiol. **71**(2), 225–229 (2000).
21. C. Chen, E. Tsina, M. C. Cornwall, R. K. Crouch, S. Vijayaraghavan, and Y. Koutalos, "Reduction of all-Trans Retinal to All-Trans Retinol in the Outer Segments of Frog and Mouse Rod Photoreceptors," Biophys. J. **88**(3), 2278–2287 (2005).
22. D. Schweitzer, L. Deutsch, M. Klemm, S. Jentsch, M. Hammer, S. Peters, J. Haueisen, U. A. Müller, and J. Dawczynski, "Fluorescence lifetime imaging ophthalmoscopy in type 2 diabetic patients who have no signs of diabetic retinopathy," J. Biomed. Opt. **20**(6), 61106 (2015).
23. C. Dysli, S. Wolf, K. Hatz, and M. S. Zinkernagel, "Fluorescence Lifetime Imaging in Stargardt Disease: Potential Marker for Disease Progression," Invest. Ophthalmol. Vis. Sci. **57**(3), 832–841 (2016).
24. Y. Geng, L. A. Schery, R. Sharma, A. Dubra, K. Ahmad, R. T. Libby, and D. R. Williams, "Optical properties of the mouse eye," Biomed. Opt. Express **2**(4), 717–738 (2011).
25. T. E. Kornfield and E. A. Newman, "Regulation of Blood Flow in the Retinal Trilaminar Vascular Network," J. Neurosci. **34**(34), 11504–11513 (2014).
26. Q. Yang, J. Zhang, K. Nozato, K. Saito, D. R. Williams, A. Roorda, and E. A. Rossi, "Closed-loop optical stabilization and digital image registration in adaptive optics scanning light ophthalmoscopy," Biomed. Opt. Express **5**(9), 3174–3191 (2014).
27. W. Becker, *The bh TCSPC Handbook,* 6th ed. (Becker & Hickl GmbH, 2015).
28. S. T. Hess, E. D. Sheets, A. Wagenknecht-Wiesner, and A. A. Heikal, "Quantitative Analysis of the Fluorescence Properties of Intrinsically Fluorescent Proteins in Living Cells," Biophys. J. **85**(4), 2566–2580 (2003).
29. N. Boens, W. Qin, N. Basarić, J. Hofkens, M. Ameloot, J. Pouget, J.-P. Lefèvre, B. Valeur, E. Gratton, M. vandeVen, N. D. Silva, Jr., Y. Engelborghs, K. Willaert, A. Sillen, G. Rumbles, D. Phillips, A. J. Visser, A. van Hoek, J. R. Lakowicz, H. Malak, I. Gryczynski, A. G. Szabo, D. T. Krajcarski, N. Tamai, and A. Miura, "Fluorescence Lifetime Standards for Time and Frequency Domain Fluorescence Spectroscopy," Anal. Chem. **79**(5), 2137–2149 (2007).
30. A. J. Walsh, J. T. Sharick, M. C. Skala, and H. T. Beier, "Temporal binning of time-correlated single photon counting data improves exponential decay fits and imaging speed," Biomed. Opt. Express **7**(4), 1385–1399 (2016).
31. C. J. Barnstable and U. C. Dräger, "Thy-1 antigen: a ganglion cell specific marker in rodent retina," Neuroscience **11**(4), 847–855 (1984).
32. G. Feng, R. H. Mellor, M. Bernstein, C. Keller-Peck, Q. T. Nguyen, M. Wallace, J. M. Nerbonne, J. W. Lichtman, and J. R. Sanes, "Imaging neuronal subsets in transgenic mice expressing multiple spectral variants of GFP," Neuron **28**(1), 41–51 (2000).
33. E. Spiess, F. Bestvater, A. Heckel-Pompey, K. Toth, M. Hacker, G. Stobrawa, T. Feurer, C. Wotzlaw, U. Berchner-Pfannschmidt, T. Porwol, and H. Acker, "Two-photon excitation and emission spectra of the green fluorescent protein variants ECFP, EGFP and EYFP," J. Microsc. **217**(3), 200–204 (2005).
34. M. Klemm, D. Schweitzer, S. Peters, L. Sauer, M. Hammer, and J. Haueisen, "FLIMX: A Software Package to Determine and Analyze the Fluorescence Lifetime in Time-Resolved Fluorescence Data from the Human Eye," PLoS One **10**(7), e0131640 (2015).
35. L. R. Ferguson, J. M. Dominguez 2nd, S. Balaiya, S. Grover, and K. V. Chalam, "Retinal Thickness Normative Data in Wild-Type Mice Using Customized Miniature SD-OCT," PLoS One **8**(6), e67265 (2013).
36. M. Y. Berezin and S. Achilefu, "Fluorescence Lifetime Measurements and Biological Imaging," Chem. Rev. **110**(5), 2641–2684 (2010).

37. R. Pepperkok, A. Squire, S. Geley, and P. I. H. Bastiaens, "Simultaneous detection of multiple green fluorescent proteins in live cells by fluorescence lifetime imaging microscopy," Curr. Biol. **9**(5), 269–272 (1999).
38. D. Magde, R. Wong, and P. G. Seybold, "Fluorescence Quantum Yields and Their Relation to Lifetimes of Rhodamine 6G and Fluorescein in Nine Solvents: Improved Absolute Standards for Quantum Yields," Photochem. Photobiol. **75**(4), 327–334 (2002).
39. T. French, P. T. C. So, D. J. Weaver, Jr., T. Coelho-Sampaio, E. Gratton, E. W. Voss, Jr., and J. Carrero, "Two-photon fluorescence lifetime imaging microscopy of macrophage-mediated antigen processing," J. Microsc. **185**(3), 339–353 (1997).
40. J. R. Lakowicz, J. Malicka, S. D'Auria, and I. Gryczynski, "Release of the self-quenching of fluorescence near silver metallic surfaces," Anal. Biochem. **320**(1), 13–20 (2003).
41. R. W. K. Leung, S.-C. A. Yeh, and Q. Fang, "Effects of incomplete decay in fluorescence lifetime estimation," Biomed. Opt. Express **2**(9), 2517–2531 (2011).
42. C. Dysli, L. Berger, S. Wolf, and M. S. Zinkernagel, "Fundus autofluorescence lifetimes and central serous chorioretinopathy," Retina **Publish Ahead of Print**(2017).

1. Introduction

High resolution *in vivo* fluorescence imaging of the retina is a powerful tool to investigate retinal structure and function in health and disease. Harnessing the contrast provided by fluorescence techniques in combination with adaptive optics, cell classes which were previously unseen in the living eye have been imaged, revealing the structure, arrangement, and morphology of different cell classes in the retina using single photon [1–6] and two-photon fluorescence [7–10]. By measuring *in vivo* changes in fluorescence intensity over time, functional responses have been seen in both monkey and mouse models using genetically encoded calcium indicators [11, 12], as well as using two-photon autofluorescence imaging in monkey [13]. Despite the utility of *in vivo* fluorescence imaging, it is difficult to disambiguate changes in fluorescence intensity, especially between imaging sessions, due to variability in factors such as fluorophore concentration, optical quality of the eye, system calibration, and photobleaching. Efforts have been undertaken to overcome these limitations by utilizing a fluorescent reference [14] or normalizing to a baseline fluorescence [13].

Fluorescence lifetime imaging has emerged as a viable technique for overcoming some of these problems, because the lifetime is an intrinsic property unique to each fluorescent molecule and its state, and is resistant to many of the factors listed above. The fluorescence lifetime is defined as the time at which the fluorescence reaches $1/e$ of its peak value through an exponential decay, following excitation by a light pulse [15]. The fluorescence lifetime is modified by the environment of the fluorophore, and therefore can be used to monitor environmental parameters such as pH, calcium, enzyme binding, or even as a marker for cell health. The structure of a molecule determines which parameters will alter its lifetime, such that not all molecules are affected by every parameter [15]. For example, the sensor pHRed has a pH-dependent fluorescence lifetime which can be used to measure intracellular pH [16].

In vivo fluorescence lifetime imaging of the retina has the potential to detect changes in cell health early in disease progression [17]. Thus far, *in vivo* fluorescence lifetime imaging of the retina has been limited to the use of standard resolution instruments that account for defocus, making it difficult to distinguish fluorophores in different layers of the retina, as well as a lack of cellular resolution and contributions to the fluorescence from the crystalline lens [18, 19]. This limitation complicates the matter of investigating diseases which affect only certain cell classes in the retina, and makes it challenging to see small, cellular level changes which may manifest early in disease progression. Furthermore, these devices have used single-photon excitation, for which the excitation light has very limited transmission below 400 nm in the primate [20], preventing excitation of fluorophores such as nicotinamide adenine dinuecleotide (NADH) and all-trans-retinol, both of which are excited maximally at ~350 nm and fall off almost entirely by 400 nm [21]. For this reason we have chosen to use two-photon excitation, which will allow for easier translation for future studies in primate. Despite the challenges inherent in single photon FLIO, the utility of fluorescence lifetime measurements has been used to show early changes in diabetic retinopathy patients and to explore the progression of Stargardt disease in the retina among other diseases [22, 23].

For the initial implementation of AOFLIO, we have chosen to image mice due to the availability of transgenic mice which express bright fluorophores in specific cells of the retina. In addition, the mouse provides optically higher transverse and axial resolution, as well as two-photon absorption efficiency, due to its high numerical aperture (0.49 – two times greater than the human eye [24]).

2. Methods

2.1 System

A new adaptive optics scanning light ophthalmoscope (AOSLO) was designed and built for two-photon imaging of the mouse eye (Fig. 1). The system is similar to the one described by Sharma *et al.* and Geng *et al.* [2, 8], but with a polygon scanner (Lincoln Laser, Phoenix, Arizona, USA) replacing the resonant scanner to provide a linear horizontal scan. The system was designed in optical design software (Code V; Synopsys, Mountain View, California, USA) to be diffraction-limited over a 5° x 5° field of view. The optical path consisted of five afocal telescopes which image the pupil of the eye through the system. All telescope pairs consisted of silver coated mirrors (JML Optical, Rochester, New York, USA) except for the final element, a 400 mm focal length, 75 mm diameter achromatic lens with broadband anti-reflection coating for 400 nm to 870 nm (Part #88598; Edmund Optics, Barrington, New Jersey, USA). The beam was de-magnified from a 5 mm system entrance pupil to the 2 mm diameter mouse pupil.

Three light sources were used for wavefront sensing and imaging. Coupled into the optical system via optical fibers were an 850 nm laser diode (Qphotonics, Ann Arbor, Michigan, USA), used for wavefront sensing, and a 790 nm superluminescent diode (Superlum, Cork, Ireland), used for reflectance imaging. The fibers were mounted on motorized stages to allow for independent focusing. A pulsed laser (Mai Tai XF-1 DS; Newport Spectra-Physics, Santa Clara, California, USA) with central wavelength tunability from 710 nm – 920 nm was used for two-photon fluorescence excitation. The laser operated at an 80 MHz repetition rate with output pulses of <70 fs. Dispersion was compensated through the use of a prism pair placed on motorized stages within the DeepSee attachment of the Mai Tai XF-1 laser. An additional glass light pipe (Part #48584; Edmund Optics) was placed at the output of the laser to bring the dispersion compensation of the DeepSee into the range required for the mouse eye. Light was focused through a spatial filter to produce a clean Gaussian beam and collimated by an achromatic doublet lens before being coupled to the entrance pupil of the AOSLO. The collimating lens was placed on a motorized translation stage to change the focus of the pulsed laser. The three light sources were combined into the system with a custom dichroic mirror (zt633_795-850tpc; Chroma Technology Corp., Bellows Falls, Vermont, USA). For all experiments in this paper, power of the pulsed laser operating at 910 nm measured at the pupil was 7 mW. Power of the 850 nm laser diode at the pupil was 35 µW, and power of the 790 nm superluminescent diode was 300 µW.

The polygon scanner scanned the light sources horizontally across the retina at a frequency of 10.8-16.2 kHz. A 2-axis tip/tilt mirror (S-334.2SL; Physik Instrumente, Karlsruhe, Germany) scanned the beam in the vertical direction and provided real-time image stabilization. The deformable mirror (DM97-08; ALPAO SAS, Grenoble, France) corrected monochromatic aberrations and controlled focus adjustment. The aberrations were measured with a Shack-Hartmann wavefront sensor using a lenslet array (Adaptive Optics Associates, Cambridge, Massachusetts, USA) with 203 µm pitch and 7.8 mm focal length placed in front of a CCD camera (Rolera XR; QImaging, Surrey, British Columbia, Canada). The deformable mirror, scanners and lenslet array were placed at planes conjugate to the entrance pupil of the mouse eye.

Backscattered light from the superluminescent diode was descanned through the system and collected through a confocal pinhole (4.3 airy-disc diameters) into a photomultiplier tube (PMT H7422-50; Hamamatsu Corporation, Shizuoka-Ken, Japan). Two-photon absorption results in axial sectioning, therefore fluorescence light emitted from the retina and transmitted through the pupil of the eye was diverted without descanning by a dichroic mirror (T660lpxrxt; Chroma Technology Corp.) and imaged onto a single photon counting detector (HPM-100-40; Becker and Hickl, Berlin, Germany). Fluorescence was collected from 400 – 550 nm, passing through two filters; one which transmitted light from 400 to 680 nm (ET680SP-2P8; Chroma), and one with a transmission window from 400 to 550 nm (E550sp-2p; Chroma). Excitation wavelength and emission filters were chosen to minimize autofluorescence. The system was completely covered and the detector baffled to reduce photon noise as much as possible.

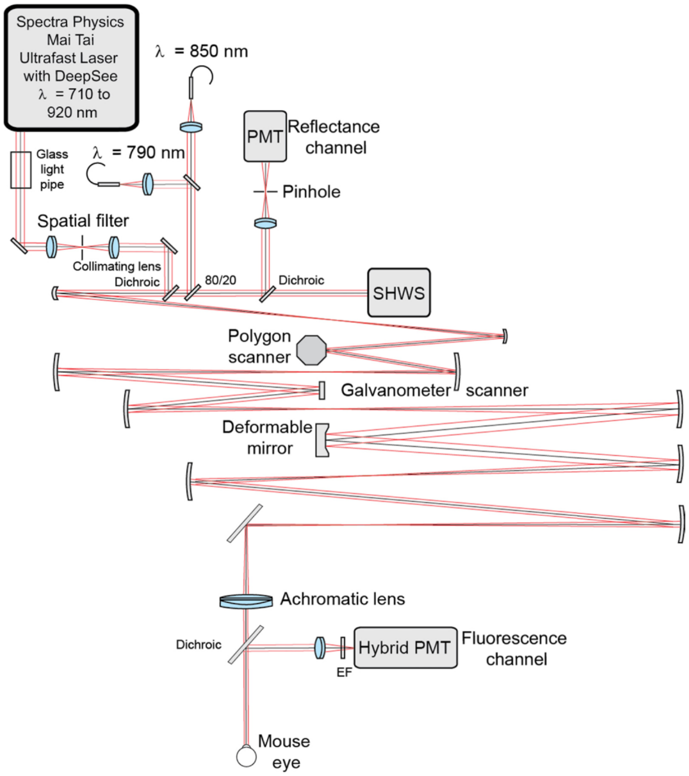

Fig. 1. System diagram of two-photon AOSLO designed for the mouse eye. PMT: Photomultiplier tube. SHWS: Shack-Hartmann wavefront sensor. 80/20: 80/20 beam splitter. EF: Emission filters.

2.2 Animal preparation

Adult Thy1-EGFP (n = 3) and C57BL/6J (n = 2) mice from 1 to 4 months of age were used in this study (The Jackson Laboratory, Bar Harbor, Maine, USA; stock #007788 and #000664, respectively). Thy1-EGFP mice are bred on a C57BL/6J background. EGFP-labeled inner retinal cells, primarily ganglion cells, were identified in Thy1-EGFP transgenic mice using low resolution fundus imaging (Micron IV; Phoenix Research Labs, Pleasanton, California, USA or Spectralis HRA + OCT; Heidelberg Engineering, Heidelberg, Germany). Mice were anesthetized with Ketamine/Xylazine injection (100 mg/kg and 50 mg/kg, respectively). For high resolution *in vivo* imaging, their pupils were dilated with a drop each of tropicamide (1%; Akorn, Inc., Lake Forest, Illinois, USA) and phenylephrine (2.5%; Akorn, Inc.) and mice were placed in a bite bar mount with a heating pad and further anesthetized with isoflurane gas (1-2%) supplemented with 98% oxygen. The details of this imaging protocol have been described fully in an earlier publication [2]. Both C57BL/6J mice, but only 1 of the

Thy1-EGFP mice were injected intraperitoneally with 0.1 mL of sodium fluorescein (10%, diluted with saline at a three-to-one ratio, for a final concentration of 3.3%; Akorn, Inc.). During imaging, each mouse was placed with its pupil at the exit pupil of the system. All experiments were approved by the University Committee on Animal Resources at the University of Rochester.

2.3 Image acquisition

The optic nerve head and vasculature present in the wide field fundus images were used to navigate to the location of interest in the AOSLO. EGFP-labeled cells which showed strong fluorescence and were near distinct vascular patterns were chosen for imaging. The excitation source for two-photon fluorescence was co-focused with the reflectance light source. The sources were focused to the uppermost vascular layer, just above the ganglion cell layer [25]. The two-photon excitation source focus was then changed slightly to bring the ganglion cells into focus. All imaged locations were within 15° of the optic nerve head. Images were acquired at a frame rate of 16 Hz. Due to breathing motion of the animal, there was noticeable motion from frame to frame prior to stabilization. A high contrast reflectance video was collected for motion estimation. Using an image-based tracking algorithm [26], the image was optically stabilized in real time by locking onto the reflectance signal focused on the vascular layer in the inner retina.

Fluorescence lifetime data was acquired using a time-correlated single photon counting (TCSPC) module (SPC-160; Becker and Hickl) [27]. A small portion of the energy in the pulsed excitation laser was sent to a fast photodiode (PHD-400; Becker and Hickl), which served as the synchronization signal for the TCSPC module. Photons were allocated in one of either 256 or 1024 time bins, depending on their arrival time with respect to the synchronization pulse. Images were acquired with 140 x 180 pixel resolution using SPCM software in First In First Out (FIFO) imaging mode (Becker and Hickl). In this mode, the TCSPC module transmits the photon data to the computer where it is then assigned to the correct pixel and time bin, allowing for larger data sets to be gathered than is possible with on-board storage [27]. Each image was acquired over 180 seconds.

2.4 Image analysis

Commercial software (SPCImage; Becker and Hickl) was used to analyze the fluorescence decay at each pixel. The instrument response function (IRF) was measured by imaging the second harmonic generation signal from urea crystals (Sigma Aldrich Corp., St. Louis, Missouri, USA) with 910 nm excitation. The IRF had a full width at half maximum of ~70 ps., which was de-convolved from the data using SPCImage. Images of vasculature labeled by sodium fluorescein were fit to a model with a single exponential decay (Fig. 2a), chosen due to negligible improvement in goodness of fit with additional terms:

$$I\left(t\right)=exp^{-\frac{t}{\tau}}+C \tag{1}$$

where *I(t)* is the fluorescence intensity at time t after the excitation pulse, τ is the fluorescence lifetime, and C accounts for background counts from the detector. Vessels were manually outlined in SPCImage software and the lifetime calculated for each pixel within a vessel. The average lifetime of all pixels in the vessel was then assigned as the lifetime for that vessel, and the overall average lifetime was a weighted average of the lifetimes of all vessels.

Cells labeled with EGFP were fit with a double exponential decay model (Fig. 2b), as found in a previous study [28]:

$$I\left(t\right)=a_1exp^{-\frac{t}{\tau_1}}+a_2exp^{-\frac{t}{\tau_2}}+C \tag{2}$$

where a_1 and a_2 are the contributions of the fast and slow lifetimes, and τ_1 and τ_2 are the corresponding lifetimes. Regions of interest were drawn around the cells and lifetimes for each pixel were calculated in SPCImage software. Lifetime values τ_1 and τ_2 were averaged in Matlab (Mathworks, Inc., Natick, Massachusetts, USA) across all pixels in the region of interest for each image. The mean fluorescence lifetime, τ_m, was calculated by:

$$\tau_m = a_1\tau_1 + a_2\tau_2 \tag{3}$$

In all displayed images, 5x5 pixels were binned around the pixel being calculated in order to increase the signal-to-noise ratio (SNR) of calculated lifetimes. In all analysis, an incomplete exponential decay model was used in order to account for long-lasting fluorescence.

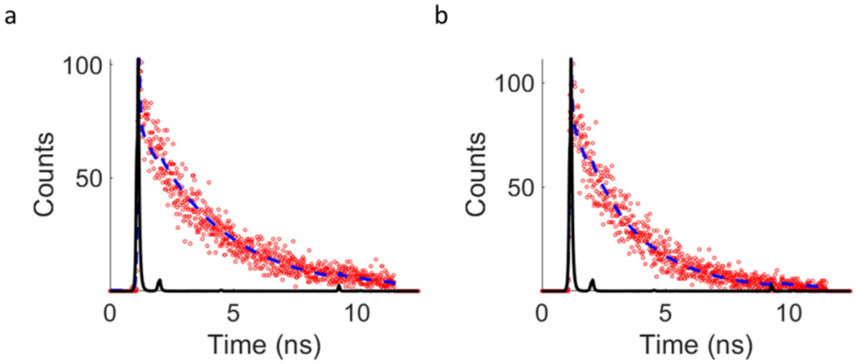

Fig. 2. Example histograms and fits for (a) fluorescein in vasculature, and (b) an EGFP-labeled cell. The red open circles correspond to the number of photons collected for each time bin. The blue dashed line shows the double-exponential fit to the data. The black solid line is the IRF of the system, which is de-convolved from the data. This fit was performed at each pixel within the image which met the threshold criteria (see section 3.2).

2.5 Statistical analysis

A Wilcoxon rank sum test was used to test for differences in the fluorescence lifetime of fluorescein between animals, and for differences in τ_1, τ_2, and τ_m of EGFP between animals. A significance value of <0.05 was used for all tests. The statistical analysis was completed in Matlab (Mathworks, Inc.).

3. Results

3.1 Imaging instrumentation calibration

The fluorescence decay of Rhodamine B (Sigma Aldrich Corp.) dissolved in methanol was measured to ensure system accuracy. When fit to a single exponential decay curve, the measured lifetime of Rhodamine B was 2.54 ± 0.25 ns (mean ± standard deviation), consistent with the results of a multi-laboratory study designed to establish fluorescence lifetime standards, which found a lifetime of 2.5 ± 0.1 ns [29].

3.2 Determination of photon threshold to calculate lifetime in a pixel

A photon threshold was set for lifetime calculation in AOFLIO images. Pixels which had less than the required number of photons were displayed in black. Photon threshold for lifetime calculation was based mainly on two factors: number of time channels acquired and number of exponentials fit to the decay. For a single exponential decay, a simulation study found that, for a 256 time channel histogram, ~500 photons are required to achieve <5% error in lifetime calculation using SPCImage [30]. We have found that the accuracy of the fit is most heavily influenced by the number of photons in the time channel with maximal number of photons (more photons results in a higher signal-to-noise ratio in each channel). Therefore, since we used 1024 time channels for the images of sodium fluorescein in vasculature, we decided to scale our threshold fourfold to 2000 photons. In general, the fluorescein fluorescence was very bright and resulted in far more photons than the threshold required.

For the images of EGFP, we used 256 time channels. The study referenced above found that approximately 4185 photons were needed to achieve a cumulative error (sum of the errors of τ_1, τ_2, a_1, and a_2) <25% for a similar fluorophore (high a_1 and $\tau_2 - \tau_1 > \sim$2ns in their case) [30]. Because of the low efficiency of two-photon fluorescence imaging through the pupil of the living mouse eye, we relaxed this constraint down to 2000 photons without substantially reducing the accuracy of the lifetime fit [30].

In order to collect the required number of photons in each pixel, we binned the decays from neighboring pixels rather than increase the image acquisition time. This is illustrated in Fig. 3, which shows the same cell from Fig. 5 with no binning, 3 x 3 binning, and 5 x 5 binning. A very low threshold of photons to calculate the lifetime was set in Fig. 3 in order to show the inaccuracy of the fluorescence lifetime calculation when too few photons are present in the decay. With no binning (Fig. 3(b)), there were too few photons in each pixel to resolve a double exponential decay, resulting in an underestimation of the cell's fluorescence lifetime and a large uncertainty. By binning each pixel with its 8 nearest neighbors (3 x 3 binning, Fig. 3(c)), the distribution of calculated lifetimes narrowed, and the mean lifetime increased to within the expected range. However, again due to the number of photons in each pixel, the fitting routine had challenges calculating τ1 and τ2, underestimating the former and overestimating the latter. By going to the 5 x 5 pixel bin (Fig. 3(d)), the distribution of lifetimes calculated within the cell further narrowed. The brightest pixel in the image now had over 5000 photons, greater than the 4185 photons found necessary to achieve <25% error in fitting by a simulation done with 256 time channels and a fluorophore with characteristics similar to EGFP [30]. As can be seen in Figs. 2(b) – 2(d), binning does reduce the spatial resolution of the lifetime image. However, there is still subcellular resolution in the lifetime image, and there is no binning in the intensity image, therefore maintaining its resolution.

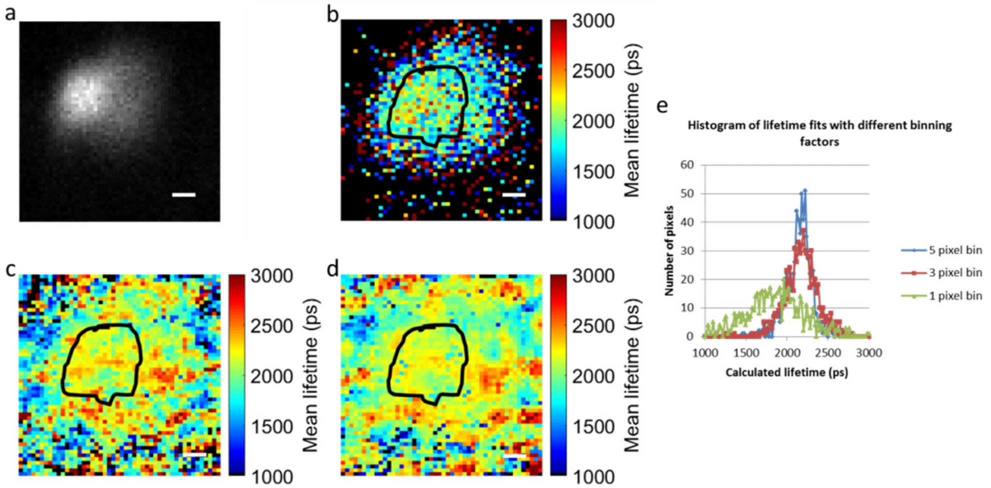

Fig. 3. Binning analysis of the EGFP-labeled cell from Fig. 5. Panel (a) shows the two-photon fluorescence intensity image of the cell. Panels (b), (c), and (d) show fluorescence lifetime images of the cell with no binning, 3 x 3 binning, and 5 x 5 binning, respectively. A very low threshold of photons was set in order to show the inaccuracy of the fluorescence lifetime calculation when too few photons are present in the decay. The black outline in panels (b), (c) and (d) indicates the boundaries of the cell, with pixels inside the outline containing greater than 2000 photons with 5 x 5 binning. Panel (e) shows histograms of the lifetime calculated at each pixel with the different binning factors shown in (b), (c), and (d). As the binning factor increases, the lifetime fit converges on the expected lifetime of EGFP. Scale bar is 5 µm.

3.3 Two-photon fluorescence lifetime imaging of sodium fluorescein in retinal vasculature

Prior to administration of sodium fluorescein, the background fluorescence level was very low (<0.02 photons/pixel/s) due to the excitation wavelength and emission filters chosen. Following injection, sodium fluorescein was present in retinal vasculature as seen in the two-photon fluorescence image shown in Fig. 4(a). A subfield of the two-photon fluorescence image was collected using TCSPC (Fig. 4(b)) and the fluorescence lifetime calculated for each pixel in the subfield (Fig. 4(c)). Vessels were then segmented manually and an average fluorescence lifetime calculated for the vessel. The mean fluorescence lifetime measured over 80 vessels was 3.21 ± 0.06 ns (Table 1). There was no significant difference in fluorescence lifetime measured across 2 mice (51 vessels in one mouse and 39 vessels in another; $p = 0.57$) or in repeated measurements in the same mouse (35 vessels in the first session and 16 in the second; $p = 0.14$).

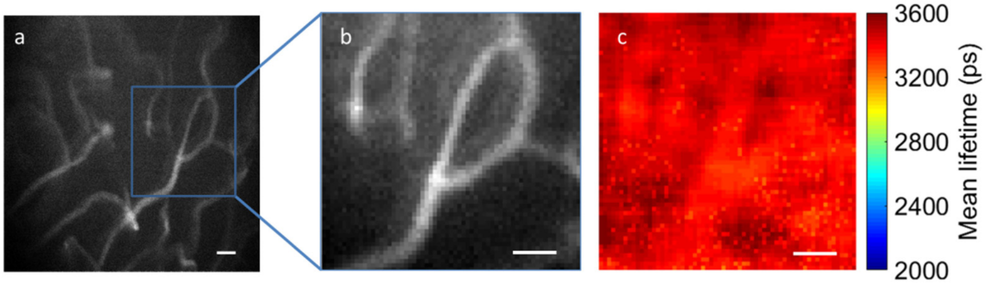

Fig. 4. Images of a capillary bed in the mouse inner retina. Panel (a) is a two-photon fluorescence intensity image acquired with a standard, analog PMT. Panel (b) is an image of a sub-portion of the location from panel (a) acquired with the single photon counting detector and the TCSPC system. The pixel density in this image is reduced compared with panel (a), however the structure of the capillaries is still visible. Panel (c) is a fluorescence lifetime image of the same location as panel (b). The fluorescence lifetime image is mostly uniform because the fluorescence lifetime is robust against intensity variations. Scale bar is 25 µm.

Table 1. Fluorescence Lifetime Values measured with AOFLIO

	Number of mice	Number of measurements	τ_1 ± SD (ns)	τ_2 ± SD (ns)	τ_m ± SD (ns)
Fluorescein	2	80 vessels	N/A[a]	N/A[a]	3.21 ± 0.06
EGFP	3	7 cells	1.43 ± 0.28	3.01 ± 0.37	2.28 ± 0.99

[a] Fluorescein data was fit with a single exponential model.

3.4 Two-photon fluorescence lifetime imaging of EGFP-labeled ganglion cells

Thy1-EGFP mice express EGFP in a sparse (<10%) subset of retinal ganglion cells [31, 32] (Fig. 5(a)). Expression and location within the mouse retina were confirmed with low resolution fundus imaging, which was also used for navigation in the small field of view AOSLO instrument. Cell somas provided the highest fluorescence signal and were often identifiable in a single frame. The SNR of a typical cell soma compared to the background noise, including autofluorescence, was ~50. The fluorescence emitted from cell somas exhibited a double-exponential decay, with the two components $\tau 1 = 1.43 \pm 0.28$ ns, and $\tau 2 = 3.01 \pm 0.37$ ns (Table 1). The mean lifetime was 2.28 ± 0.99 ns, and was consistent throughout the soma of the cell (Fig. 5(c)). There was no significant difference in τ_1, τ_2, or τ_m across 7 cells in 3 mice ($p = 0.7, 0.8, 0.4$, respectively). The fluorescence signal from axons was much lower, and they became visible only after summing a large number of frames. Fluorescence emitted from dendrites and axons did not yield the required number of photons to calculate lifetime.

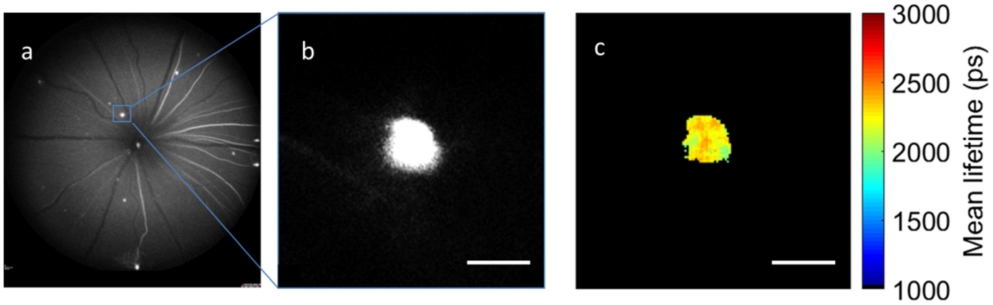

Fig. 5. Images of an EGFP-labeled ganglion cell in a Thy1-EGFP mouse retina. Panel (a) shows sparse EGFP labeling of cells and axons in the mouse retina. The blue box denotes the region of AOFLIO imaging which is shown in panel (b). Panel (b) is a two-photon fluorescence intensity image of a ganglion cell soma. The same fluorescent axon can be seen in panels (a) and (b). Panel (c) is a fluorescence lifetime image of the same location. The lifetime calculated was consistent throughout the soma of the cell, despite the intensity of fluorescence changing throughout. The fluorescence lifetime was not calculated in the axon because it did not reach threshold criteria. Scale bar is 25 µm.

3.5 Simultaneous two-photon fluorescence lifetime imaging of EGFP-labeled ganglion cells and sodium fluorescein

A Thy1-EGFP mouse was first placed in the system and a ganglion cell imaged to measure the fluorescence lifetime. The mouse was then injected with sodium fluorescein. In the resulting fluorescence image, fluorescence originated from both the EGFP in the ganglion cell and the sodium fluorescein in the surrounding capillary bed (Fig. 6(c)). The cell was indistinguishable in the fluorescence intensity image, and could not be spectrally filtered because EGFP and sodium fluorescein have nearly identical emission spectra (Fig. 6(b)) [15, 33]. Because of their different fluorescence lifetimes, we were able to identify the cell using fluorescence lifetime imaging (Fig. 6(d)). The cell was most easily identifiable by looking at the contributions from the fast and slow portions of the fluorescence lifetime when τ_1 and τ_2 were set to the known lifetimes (from previous measurements in sections 3.3 and 3.4) of EGFP and sodium fluorescein, respectively. Because the long lifetime component of EGFP was similar to the lifetime of fluorescein fluorescence, we considered a two-component fit. The mean lifetime for each pixel was then displayed, and showed a lower value in the region of the cell. By multiplying the intensity image (I(x,y)) by the contribution from the fast (a1(x,y)) or slow (a2(x,y)) lifetime at each pixel two images can be obtained. The image containing the fast lifetime component results in the cell becoming visible (Fig. 6(e)), whereas the image containing the slow lifetime component improves the contrast of the vessel, due to reduced contribution from the cell (Fig. 6(f)).

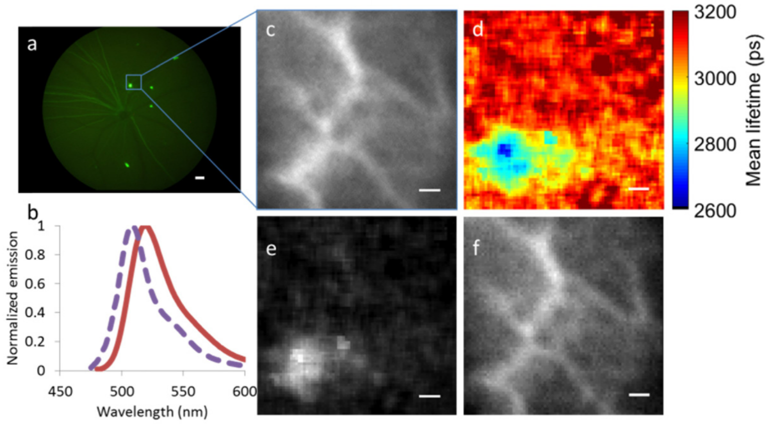

Fig. 6. - Images of an EGFP-labeled cell surrounded by a bed of capillaries with fluorescein. Panel (a) shows the wide field image of the ganglion cell and its axon connecting to the optic nerve. Panel (b) shows the overlapping emission spectra for EGFP (purple dashed line) and fluorescein (red solid line), acquired from Chroma Technology Corp. Panel (c) shows the two-photon fluorescence intensity image; the cell is indistinguishable from the vessels. Panel (d) shows the fluorescence lifetime image. The EGFP fluorescence from the cell exhibits a lower fluorescence lifetime than the fluorescein, revealing the location of the cell. Panels (e) and (f) are intensity images which have been scaled by a1(x,y) (the contribution of the fast lifetime component) or a2(x,y) (the slow lifetime component), respectively. The fast lifetime component corresponds to EGFP fluorescence, causing the cell to appear in (e), while the slow lifetime component corresponds to the fluorescein, suppressing the cell in (f) and improving the vessel contrast. Scale bar is 100 µm for panel (a) and 15 µm for panels (c) – (f).

4. Discussion

The mouse eye provides an ideal testbed for AOFLIO. Previous reports of FLIO have mostly focused on the human eye, but due to the low numerical aperture of the eye, high absorption of blue light by the crystalline lens, and lack of adaptive optics, it has been challenging to isolate fluorescence from single cells in the retina, and correction factors have had to be made for fluorescence from the crystalline lens [17, 34]. The advantage in focusing power provided by the high numerical aperture of the mouse eye, as well as the use of adaptive optics to optimize the point spread function, allows us to image individual cells. Based on previously reported axial resolution in a mouse AOSLO, we estimate the axial resolution of our system to be ~18 µm [2]. The thickness of the nerve fiber layer in the wild type mouse was found to be 19 µm on average [35]. As we are focused in the ganglion cell layer, we reduce fluorescence contributions from the lens or other retinal layers interfering with the fluorescence signal.

Adaptive optics image quality in the mouse can vary drastically between imaging sessions. Because the fluorescence lifetime is less affected by these parameters (for example, it is largely independent of fluorescence intensity or fluorophore concentration [36]), it may be less dependent on image quality than measures which depend on the optical quality (ex. Image-based metrics), an important factor for longitudinal imaging studies. In Fig. 4(b), a slight motion blur can be seen in the vessel. The number of photons outside of the vessel, which may be due to the motion blur or out of focus fluorescence from another vessel layer, is far fewer (~3x greater in the vessel), but the lifetime calculated is very similar. In addition, fluorescence lifetime imaging can provide quantitative measurements, rather than relying on relative changes as is the case in many ratiometric fluorescence techniques. In this study we found no differences in fluorescence lifetime across cells (in the case of EGFP) or vessels (in the case of fluorescein), despite differences in image quality between images.

The fluorescence lifetime of EGFP that we measure *in vivo* is comparable to that previously measured in vitro by other groups [28, 37]. The lifetime of fluorescein that we measured was lower than the ~4 ns reported by other groups [38, 39]. We speculate that this is due to the high concentration of sodium fluorescein used in this study, which can result in self-quenching, which occurs when the energy of an excited state molecule is transferred to a non-fluorescent trap during the process of resonance energy transfer [40]. This is a well-known property of fluorescein which can cause reduced quantum yield and fluorescence lifetime.

As compared with two-photon fluorescence imaging, where we can acquire images with greater than 500 pixels in each linear dimension, we lose resolution when acquiring fluorescence lifetime images. A consequence of our fast scanning rates (resulting in pixel dwell times of ~25 ns for a 500 pixel linear dimension), is that we must downsample our AOFLIO images. This is because the acquisition software does not allow for shorter than a 100 ns pixel clock when generated internally, and if we provide our own external pixel clock, it alone saturates the TCSPC card data transfer to the computer, preventing photon data from being transferred and sometimes crashing the acquisition program. This downsampling results in images with only 140 x 180 pixel resolution. At this pixel resolution, the pixel size is approximately the same size as the diffraction-limited spot size, meaning that we are sampling below the Nyquist limit in this implementation. By reducing the number of pixels acquired, there is a higher probability of a photon being detected in each pixel, leading to a higher number of photons per pixel. This allows for a higher SNR for the lifetime decay calculated for each pixel. In addition, spatial binning of the data improves the accuracy of the lifetime calculation, but reduces the spatial resolution of the lifetime image by introducing blur. Alternatively, it is possible to increase the number of photons in each pixel by lengthening the image acquisition time. However, we chose to limit our acquisition to 180 seconds due to concerns about photodamage from increased exposure time.

AOFLIO is well-suited to image fluorophores typically encountered in retinal imaging; their lifetimes range from ~0.5 ns (free NADH) to ~4 ns reported previously for measurements of fluorescein [38]. With an IRF of only ~70 ps, a lifetime of 0.5 ns can be easily measured. The upper bound of measurement is 12.5 ns, which corresponds to the period of the pulsed laser used for fluorescence excitation. It is important to note that the true upper bound of measurement is probably much lower, as the fluorescence has only decayed to its 1/e value at the time calculated to be the fluorescence lifetime – therefore, a fluorescence lifetime near the pulse period of the laser would result in contributions to the fluorescence from previous excitation pulses. To mitigate this effect, we used an incomplete exponential decay model [41].

As demonstrated, we show it is possible to distinguish fluorophores in the retina with similar spectra via their fluorescence lifetime. This has great potential as the number of spectrally separable channels in visible fluorescence is limited by the spectral specificity and overlap of a fluorophore with its spectral neighbors. This is particularly important for imaging the outer retina, where both NADH and fluorescent retinoids reside. These molecules have similar excitation and emission spectra, making it challenging to separate them with traditional fluorescence imaging [21]. The ability to separate fluorescence contributions from these fluorophores by their lifetime could help mitigate confounding factors in studies of the visual cycle involving retinoid fluorescence [13] or prospective studies of photoreceptor health. As with intensity-based imaging methods, differentiating fluorophores based on lifetime requires that the emitted fluorescence intensities be of similar order of magnitude, otherwise the signal from the stronger fluorophore would overwhelm any signal from the weaker fluorophore.

In this paper we combine two-photon adaptive optics scanning light ophthalmoscopy with fluorescence lifetime imaging ophthalmoscopy (FLIO). In comparison to existing literature [17, 19, 22, 23, 42], we demonstrate two advantages. By using adaptive optics we are able to correct the aberrations induced by the eye and provide a tighter focus both laterally and axially, allowing us to resolve single cells. In addition, the use of two-photon fluorescence provides a clear path to translation to the primate eye, which blocks nearly all light below 400 nm [20]. This capability will allow AOFLIO of fluorophores involved in cellular processes that cannot be excited with single photon excitation [9, 10]. Conversely, single photon FLIO using a modified clinical device is able to image a 30° field of view, providing it with the ability to rapidly assess large-scale changes in the retina.

The ability to measure fluorescence lifetime on a cellular scale in the living eye provides a sensitive measure of cell health. This technique could be used to evaluate vision restoration therapies such as stem cells or antioxidant therapy. By measuring the fluorescence lifetime, it may be possible not only to determine whether cells are alive, but also whether they are functioning normally. This could be done using fluorescently labeled molecules or by measuring the fluorescence lifetime of intrinsic fluorophores such as NADH. AOFLIO with intrinsic fluorescence is likely to require longer acquisition times due to lower concentrations and reduced fluorescence efficiency of these fluorophores.

5. Conclusion

In this first implementation of AOFLIO, we have demonstrated its functionality in imaging several extrinsic fluorophores in the retina. Future applications of this technique will uncover information about the environment of key fluorophores involved in cellular metabolism and the visual cycle. Furthermore, by utilizing exogenous fluorophores that can be inserted in the mouse retina, we are able to increase our specificity by targeting specific molecules that may be indicators of cell health. With further improvements, this technique may be deployed to study progression of disease.

Funding

National Institutes of Health (NIH; EY022371, EY001319, EY007125, EY025497); Research to Prevent Blindness.

Disclosures

JAF: Polgenix, Inc. (F), University of Rochester (P); JJH: Polgenix, Inc. (F), University of Rochester (P).

Acknowledgements

We would like to thank Qiang Yang, Martin Gira, Keith Parkins, Jennifer Strazzeri, Daniel Guarino, and Jesse Schallek for their assistance with the project. Alfredo Dubra and Kamran Ahmad developed the adaptive optics control software.